Fast synthesis of the iridium(III) complexes at room temperature for high-performance OLEDs

参赛队员：张知为

指导教师：郑佑轩 许亮亮

指导学校：南京大学、南京外国语学校

本参赛团队声明所提交的论文是在指导老师下进行的研究工作和取得的研究成果。尽本团队所知，除了文中特别加以标注和致谢中所罗列的内容以外，论文中不包含其他人或本团队已经发表或撰写过的研究成果。若有不实之处，本人愿意承担一切相关责任。

参赛队员签名：张知为

日 期：2019 年 9 月 1 日

Abstract:

Organic light-emitting devices (OLEDs) have attracted much attention due to their advantages of low driving voltage, high brightness and high efficiency. They have broad application prospects in solid-state lighting and flat panel display. Among the emitters used in OLEDs, the iridium(III) complexes have been widely applied due to their tunable emission energy, excellent chemical stability and high photoluminescent efficiency. But for the preparation of most Ir(III) complexes, the last reaction process is always kept at high temperature for a long time, which would inevitably increase the manpower and cost. Therefore, it is important to find suitable ligands which can form phosphorescent complexes at room temperature efficiently. In this paper, a sulfur atom containing ligand of *N*,*N*-diisopropyl dithiocarbamate was prepared and used as an ancillary ligand for red and green Ir(III) complexes with 4-(4-(trifluoromethyl)phenyl)quinazoline and 2-[4-(trifluoromethyl)phenyl]pyridine as the cyclometalated ligands, respectively. Both complexes were synthesized at room temperature in few minutes and also show good device performances. Respectively, the red OLED shows a maximum luminance above 26000 cd m^{-2} and an EQE_{max} of 15.30%. and the green device displays a L_{max} above 33466 cd m^{-2} with an EQE_{max} of 25.17%. These results suggest that the sulfur containing Ir(III) complexes have potential application in OLEDs with reduced cost.

Key words: organic light-emitting diodes, high-efficiency, fast room-temperature synthesis, iridium complexes, red and green light.

1. Introduction

1.1 Concept of electroluminescence and advantage of organic light-emitting diode (OLED).

Electroluminescence (EL) is a process by which photons are generated when the excess electron–hole pairs are created by an electric current caused by an externally applied bias. And the organic light-emitting diode (OLED) is the device which can realize the EL process. Nowadays, the display market is predominated by LCD (liquid crystal display). But LCD has its weaknesses like slow response time, requirement for the background light, high cost of energy, narrow viewing angle and instability to high temperatures, which provides the chance for the rise of OLEDs. Currently, OLED has taken quite a place in the mobile display market and also begun expanding their presence to TVs market and lighting with a near-30-year development, including the potential for flexible screen.

1.2 Working mechanism of OLED

The typical electroluminescence device consists of glass substrate, transparent anode, electron hole transport layer, emissive layer, and cathode, etc. Figure 1 provides an example of the electroluminescence device and illustrates the steps of illumination.

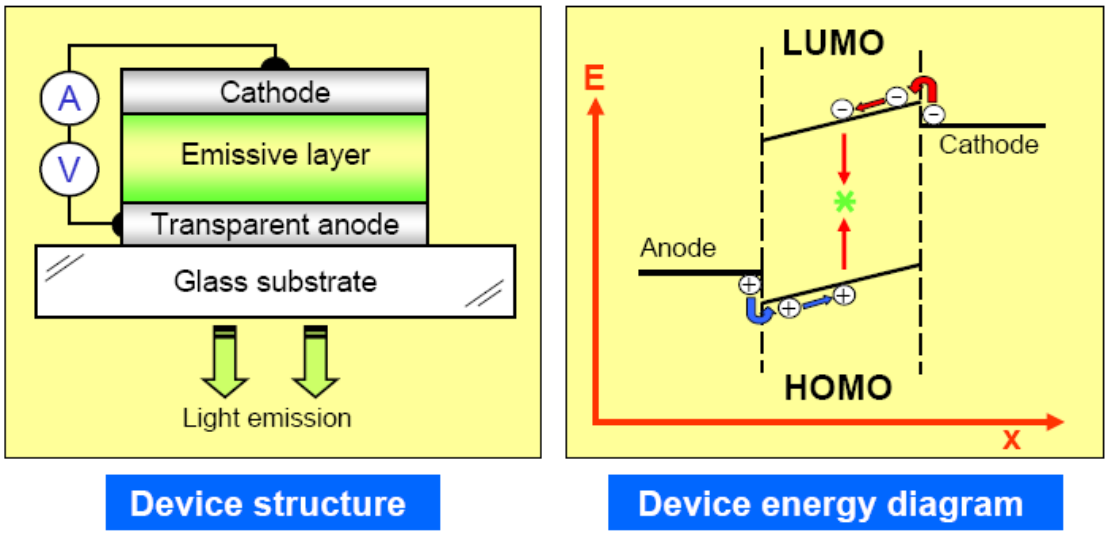

Figure 1. The OLED structure and its working mechanism.

① Holes and electrons are filled the highest occupied molecular orbit (HOMO) and

the least unoccupied molecular orbit (LUMO) from the anode and the cathode in the action of the electric field exerted on the device in the active layer.

② Holes in HOMO and electrons in LUMO become closer to each other.

③ Electrons in LUMO and holes in HOMO of organics combine with each other in the emissive layer to form excitons.

④ Finally, the energy of the excitons are transferred to the emitters to make luminescence.

1.3 Emitters for OLED devices

As emitters in OLED, there are mainly three types of materials (Figure 2). After the birth, excitons in organic molecules come to the singlet excited state (S_1, S_2……) from the ground state (S_0). Meanwhile, the instable high-state excitons drop back to the minimum excited state S_1 by internal conversion, and the electrons in state S_1 have the possibility of reaching the triplet state with the least energy T_1 by intersystem crossing. If the electron goes back to S_0 (electronic ground state) from S_1 in the form of electromagnetic radiation, the material gives out fluorescence. What's more, according to Statistical theory of electron spin and quantum chemistry, the proportion of singlet excitons and triplet excitons turns out to be 1:3. But because in most of the molecules, the triplet excitons are prohibited from going back to the ground state or giving out phosphorescence (they would turn into heat), which cause the maximum efficiency of OLED device to nearly 25%.

If the electron goes back from T_1 to S_0, phosphorescence would take place. However, due to the fact that the spin direction of the electron on S_0 varies from that on the T_1, phosphorescence couldn't be obtained because of forbidden transition generally. But in complexes with the heavy-metal center, the existence of heavy-metal atoms causes spin-orbital coupling (SOC), making the prohibited triplet able to give phosphorescence and improving the efficiency of the device to 100%. At present, the cyclometalated iridium(III) complexes have attracted great attention because of their tunable emission energy, excellent chemical stability and high photoluminescent efficiency [1]. For the commercial OLED products, the green and red emitters are Ir(III) complexes. But in

comparison with extensively studied Ir(III)-based red and green phosphorescent complexes, the efficient blue emitters are limited due to their high lying energy level and long triplet state lifetime, and the performances of blue OLEDs are still not satisfactory. Therefore, achieving stable and highly efficient blue phosphorescent Ir(III) complexes and their corresponding devices still remains a significant challenge with low device operation lifetime.

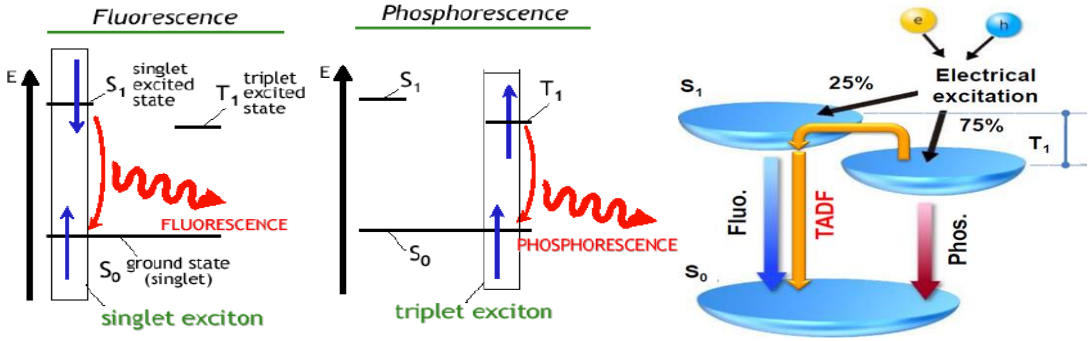

Figure 2. The luminescence mechanisms of three type materials.

The recent breakthrough of Thermally Activated Delayed Fluorescence (TADF), first reported by C. Adachi et.al. [2], symbolizes a huge leap for OLED because it endows pure organic compounds with the capability to maximize the efficiency of exciton harvesting to 100%. Owing to the small band gap between S_1 and T_1 (ΔE_{ST}) states of these materials, the reverse transferring process from T_1 to S_1 is drastically accelerated, leading to 100% of energy utilization during electroluminescence process. To minimize the ΔE_{ST}, the most common strategy is to introduce spatially separated HOMO and LUMO dominated moieties without compromising the oscillating strength (e) between S_1 and S_0 state. This strategy has been validated many times towards realization of highly efficient TADF characteristics, and numerous OLEDs bearing this concept have been fabricated with decent performances, which have potential application for blue devices. But the drawback of TADF materials is that the lifetime of T_1 state is still too long in most cases, which also reduce their device stability and operation lifetime. Therefore, for the commercial OLED products, the blue emitters are still fluorescence materials, which affect the efficiency of the OLEDs.

1.4 The development of Ir(III) complex

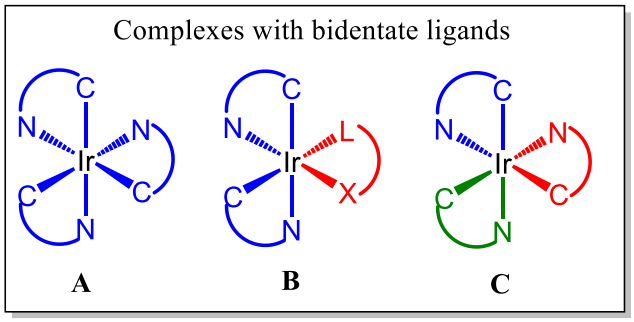

Figure 3. Different coordination types of neutral Ir(III) phosphorescent complexes (C^N: main ligand, L^X: ancillary ligand).

As mentioned in the Figure 3, the phosphorescent Ir(III) complexes adopt a disordered octahedral geometry with six coordination bonds. For complexes with structures **A**-**C**, three monovalent bidentate ligands are used to form homoleptic (**A**) complex with same organometallic ligands and heteroleptic (**B** and **C**) complexes with different ligands. Normally, Ir(III) complexes used in OLEDs are divided into three main groups depending on the light they give off when exerted with electric current: green, red and blue Ir(III) complexes (some examples are listed in Figure 4). Since the emitting properties of the Ir(III) phosphors are mainly determined by the triplet metal-to-ligand charge transfer state (^{3}MLCT) and/or triplet ligand centered charge transfer state (^{3}LC), the energy levels and the ligand field strength of the organometallic ligands are essential for the emission color, band width, decay time and quantum yields, etc.

The research on the green complexes were done the earliest because they always show higher brightness and efficiency than the other two kinds. The most widely and intensively studied green Ir(III) complex is *fac*-Ir(ppy)$_3$ whose application in the organic electrophosphorescent device was first reported by Thompson and Forrest et al. in 1999 [3]. Due to the proper ligand filed strength and energy level of ppy derivatives, many efficient green homoleptic Ir(III) phosphors have been developed in the past years. But the synthesis of homoleptic Ir(III) is complicated due to the high synthesis temperature and mixed products of *fac/mer*-Ir(ligand)$_3$, which were difficult to be separated. Therefore, most work were focusing on the heteroleptic Ir(III) complexes

with different ancillary ligands. The most widely used and intensively studied ancillary ligand is acetyl acetone (acac), such as $Ir(ppy)_2(acac)$ [4]. Since the acac ligand does not exert significant influence on the frontier molecular orbitals, the photophysical properties of the heteroleptic phosphors with acac ancillary ligand are mainly determined by the main organometallic ligands. In 2011, Zheng Youxuan group reported a novel ancillary ligand tetraphenylimidodiphosphinate (tpip) with large steric hindrance and the corresponding phosphor $Ir(tfmppy)_2(tpip)$ has good electron mobility [5]. Consequently, the device efficiency can be enhanced and the efficiency roll-off effect can be suppressed.

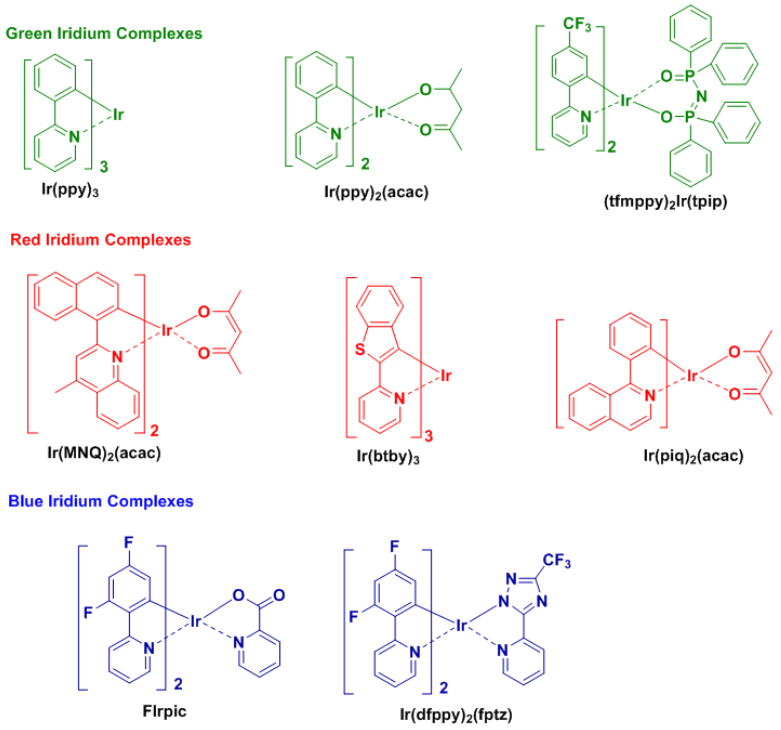

Figure 4. The examples of some iridium(III) complexes with green, red and blue colors.

Red Ir(III) complexes come after the green ones. In order to achieve long wavelength emission, the phosphors should have small HOMO/LUMO energy band gap, which guarantees the low emissive excited state energy. The widely-used molecular design approaches are increasing the conjugated structure of the organometallic ligand by fused aromatic rings and introducing electron-rich aromatic moieties into the ligand, such as the complexes of $Ir(btby)_3$, $Ir(MNQ)_2(acac)$ and $Ir(piq)_2(acac)$.[4]

But in comparison with extensively studied Ir(III)-based red and green

phosphorescent complexes, the efficient blue emitters are limited due to their high lying energy level and long triplet state lifetime, and the performances of blue OLEDs are still not satisfactory. As the most famous sky-blue emitter, FIrpic benefits from not only the fluorine substituents on the ppy main ligand but also the pic ancillary ligand with high ligand field strength. By replacing pic by 1,2,4-triazole pyridine, $Ir(dfppy)_2(fptz)$ derivatives were also widely investigated [6]. Therefore, achieving stable and highly efficient blue phosphorescent Ir(III) complexes and their corresponding devices still remains a significant challenge with low device operation lifetime.

1.5 The research target of this work

As mentioned before, the Ir(III) complexes are the most important emitters for OLEDs, and the demand for this precious substance is huge in the industrialization of product. In order to speed up the process of OLEDs industrialization, cost reduction is also important. But for the preparation of most Ir(III) complexes, the last reaction process is always to reflux the $[(C\text{^}N)_2Ir(\mu\text{-}Cl)]_2$ chloride-bridged dimmer with cyclometalated or ancillary ligands at high temperature (110 ^oC) for a long time (> 2 h), which would inevitably increase the manpower and cost. It is important, but difficult to find suitable ligands which can form phosphorescent complexes at room temperature efficiently to reduce the cost of OLEDs industrialization significantly.

Meanwhile, four-membered ring structures of Ir(III) complexes with sulfur atoms in the ancillary ligands are rarely studied in OLEDs, and there is no new progress in the research of the Ir(III) complexes containing the four-membered ring based on Ir-S-C-S backbone. Furthermore, the Hard-Soft-Acid-Base (HSAB) theory is widely used to judge the stability of the metal complexes and also to explain the reaction mechanism. The central theme of this theory is that when all other factors are the same, the "soft" acid with the "soft" alkali and the "hard" acid with the "hard" alkali react more quickly and form strong bonds. Based on this theory, the central iridium atom and sulfur ion can be classified as soft acid and base, respectively, thus the bonding speed of complexes is fast and the formed compounds are stable. Therefore, in this paper we synthesize two red and green Ir(III) complexes at room temperature in several minutes with the sulfur-containing ligands.

2. Rapid synthesis of a red iridium(III) complex with four-membered Ir-S-C-S chelating ring at room temperature

2.1 Preface

The idea of introducing organic materials into OLED was first proposed by Dr. Ching. W. Tang in 1987. In recent years, considerable attention has been caught by OLEDs due to their successful applications in solid-state lighting and full-color flat-panel display. Phosphorescent materials utilize both the singlet and triplet excitons by SOC effect because of the heavy metal atoms existing in the molecule, leading to the internal quantum efficiency of 100%. Emitting materials with iridium atoms stand out in terms of their properties with short excited lifetime (microsecond time-scale), color tuning flexibility, high quantum yields and thermal stability. But for the production of most Ir(III) complexes, the last reaction process is always to mix chloride-bridged dimmer with cyclometalated or ancillary ligands at high temperature for a long time, which would inevitably increase the manpower and cost. To further improve the ease of manufacturing and lower the energy cost, rapid synthesis of Ir(III) complex at room temperature is a significant challenge. Ancillary ligands usually consist of atoms like carbon, nitrogen and oxygen, but sulfur atoms are rarely introduced to auxiliary ligands and used in the OLED materials. For the previously reported Ir(III) complexes, ancillary ligands mainly formed six or five-membered ring structures. But the Ir(III) complexes containing four-membered ring structures make the angle formed by the two coordinated atoms of the ancillary ligand and the iridium atom much reduced, suggesting the four-membered metallocycles would possess greater coordination strain energy. However, four-membered ring structures of Ir(III) complexes with sulfur atoms in the ancillary ligands are rarely studied in OLEDs, and there is no new progress in the research of the Ir(III) complexes containing the four-membered ring based on Ir-S-C-S backbone.

With this consideration, sulfur atoms with electron-donating groups forming ligands such as N,N-diisopropyl dithiocarbamate (dipdtc) are added into the Ir(III) complexes, mixing with the electron-deficient 4-(4-(trifluoromethyl)phenyl)quinazoline (4tfmpq) moiety as the cyclometalated ligand .

2.2 Experimental

All chemical reagents are purchased commercially without purification. NMR is measured in Bruker AM 400M, molecular masses of the ligands are measured by ESI-MS (LCQ fleet, Thermo Fisher Scientific). Molecular mass of the complex is measured on MALDI-TOF-MS. Elemental analyses of the percentage of carbon, nitrogen and oxygen are completed on Elementar Vario MICRO analyzer. Thermal analysis is tested on DSC 823e analyzer (METTLER). Absorption and emission spectra are measured respectively on UV-3100 and Hitachi F-4600. Lifetime for the complex is tested in normal temperature and anaerobic system, using Edinburgh Instruments FLS-960. Electrochemistry statistics are measured on MPI-A multifunctional electrochemistry and chemical luminance instrument with tetrabutylammonium hexafluorophosphate as supporting electrolyte, ferrocene as external standard, glassy carbon electrode as electrode, platinum wire electrode as the opposite electrode, and Ag/$AgNO_3$ electrode as the reference electrode. Quantum efficiency of the solution is calculated by comparing the strength of the emission peak of the sample and the standard *fac*-Ir(ppy)$_3$ in the formula below:

$$\Phi_s = \Phi_{std}\left(\frac{I_s}{I_{std}}\right)\left(\frac{A_{std}}{A_s}\right)\left(\frac{\eta_s}{\eta_{std}}\right)^2$$

2.2.1 Reagents

4-Trifluoromethylphenylboric acid, 4-chloroquinazoline, diisopropylamine, LiOH•H_2O, benzene, $IrCl_3$, anhydrous THF, 2-ethoxyethanol ($EtOCH_2CH_2OH$) and Pd(PPh_3)$_4$.

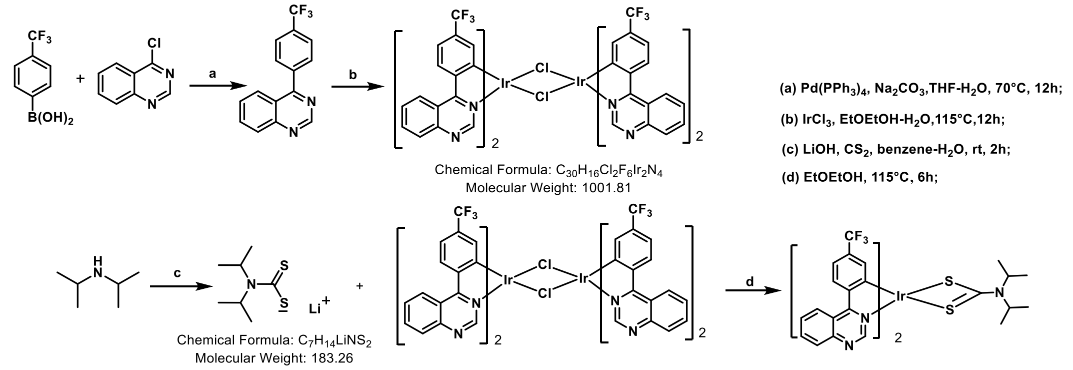

Scheme 1. Synthetic routes of ligands and red Ir(III) complex.

2.2.1 Synthesis of 4-[(4-trifluoromethyl)phenyl]quinazoline

Put 4-trifluoromethylphenylboric acid (2.5 mmol, 0.48 g), 4-chloroquinazoline (2.5 mmol, 0.42 g) and $Pd(PPh_3)_4$ (2.5 mmol, 2.8 g) into the reaction container under nitrogen for protection, and the solution was heated at 70 ^oC for 12h. Separated the liquid mixture after extraction to get 4-[(4-trifluoromethyl)phenyl]quinazoline (0.9 mmol, 0.25 g), with a yield of 36%.

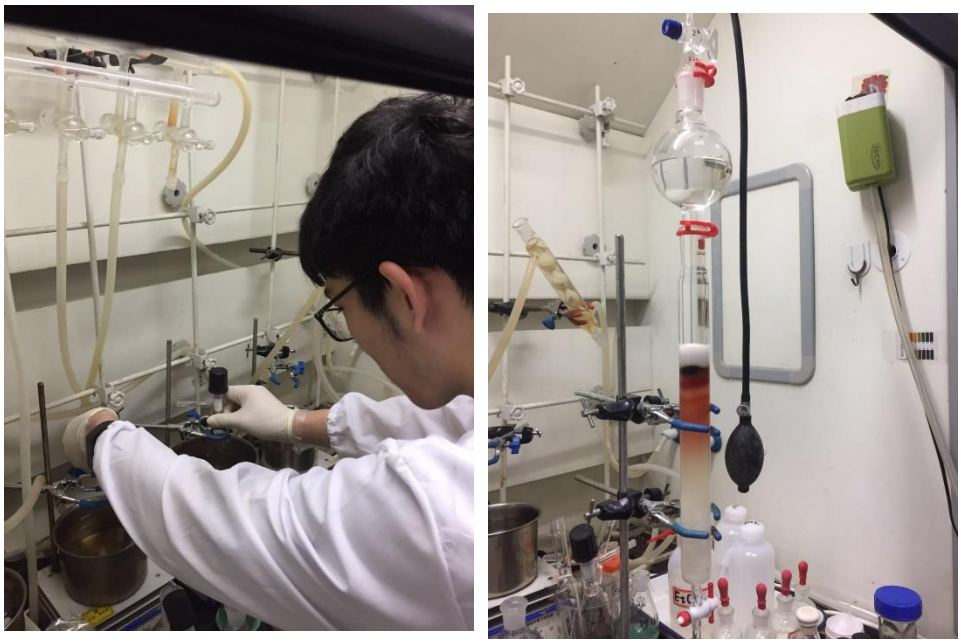

Figure 5. Synthesis of 4-[(4-trifluoromethyl)phenyl] quinazoline.

2.2.2 Synthesis of dithioformate

Figure 6. Synthesis of dithioformate

Into a three-mouth flask, water (3 mL), benzene (10 mL) and $LiOH•H_2O$ (1.0 g, 24

mmol), CS_2 (1.8 g, 24 mmol) were added at room temperature, and the mixture was stirred without nitrogen protection. Diisopropylamine (2.0 g, 20 mmol) was then added in drops. The reaction slowly releases heat and form yellow precipitation, which turned to orange after 60 minutes. After 60 minutes, petroleum ether was added to precipitate all products, which were vacuum filtered and washed with petroleum ether .

2.2.3 Synthesis of iridium chloride bridge dimmer

Put 4-[(4-trifluoromethyl)phenyl]quinazoline (0.25 g, 0.9 mmol), $IrCl_3$ (0.10 g, 0.36 mmol), $EtOCH_2CH_2OH$ (10 mL) and water (5 mL) into three-mouth flask. The solution was heated at 115 ^oC for 12h. Then, cooled the flask down and added water to form the precipitation, which was filtered and washed with dichloromethane (0.06 g).

Figure 7. Synthesis of the iridium chloride bridge dimmer

2.2.4 Synthesis of the complex.

Figure 8. Synthesis of the complex.

The complex was obtained by reaction of iridium chloride bridge dimmer with substituted dithiocarbamate. Add the chloride bridge dimmer (0.06 g, 0.038 mmol), dithioformate (0.03 g, 0.152 mmol) and $EtOCH_2CH_2OH$ (15 mL) into the three-mouth flask, and the solution was stirred for 5 minutes at room temperature. The solution was extracted with CH_2Cl_2 and water, dried with anhydrous Na_2SO_4. After removing the solvent in vacuum, the residue was purified by chromatography with eluent (CH_2Cl_2 : petroleum ether = 2:1) and obtained red solid 274 mg with a yield of 72.0%, which was further purified by vacuum sublimation. Because of the red light it gave off under UV light, we name it ***Ir**red* in the following research for convenience. ^1H NMR (400 MHz, $CDCl_3$) δ 10.44 (s, 2H), 8.85 (d, *J* = 8.51 Hz, 2H), 8.43 (d, *J*= 8.46 Hz, 2H), 8.32(d, *J* = 8.03 Hz, 2H), 8.02 (ddd, *J* = 1.17, 7.03, 8.33 Hz, 2H), 7.86 (ddd, *J* = 1.19, 7.01, 8.36 Hz, 2H), 7.19 (dd, *J* = 1.42, 8.47 Hz, 2H), 6.75 (s, 2H), 1.32 (d, *J* = 54.11 Hz, 14H). HR-MS, m/z: calcd for $C_{37}H_{30}N_5F_6S_2Ir$, 915.1476 [M]; found 916.1557 $[M+H]^{+\cdot}$ Anal. Calcd for $C_{37}H_{30}N_5F_6S_2Ir$: C, 48.57; H, 3.30; N, 7.65. Found: C, 48.67; H, 3.32; N, 7.75%.

Figure 9. The complex in solution under UV light.

2.3 Results and discussion

2.3.1 Analysis of the structure of ***Ir**red* single crystal.

The single crystal was obtained by vacuum sublimation and X-ray diffraction measurements was carried out. The ellipsoid structure is shown in Figure 10. Crystal parameters and bond length and bond angle data are shown in the Table 1 and 2.

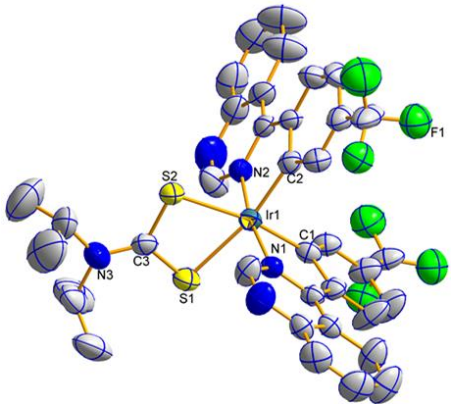

Figure 10. The ellipsoid structure of the complex ***Ir**red* (hydrogen omitted), (CCDC No. 1832357) .Ellipsoids are drawn at 50% probability level.

The expected octahedral coordination geometry is formed with iridium atoms as the center which has six coordination sites. Structurally, in ***Ir**red*, two coordination C atoms of main quinazoline ligands are on one side of the iridium atom, causing the [C1-Ir-C2] angle less than 90 degrees, while two N atoms form a straight line on both sides of the iridium atom. The ***Ir**red* has octahedral coordination geometry around iridium center by three chelating ligands with *cis*-C-C and *trans*-N-N dispositions in which the N-Ir-N angles is almost 175°. Two coordination S atoms and two coordination C atoms form a planar quadrilate-like structure. The four-membered Ir-S-C-S backbone could cause significantly acute S-Ir-S bite angle compared with the larger five-membered or six-membered heterocycles based on such as pic, acac derivatives. It also illustrates that -1 charge of dithiocarbamate is scattered over both sulfur atoms. The two coordinated S atoms of ancillary ligand reside in the equatorial plane *trans* to the metalated atoms. From the above analysis, this compact and tensile bonding mode is well understood.

Table 1. Crystallographic data of ***Ir**red*.

	***Ir**red*
Formula	$C_{37}H_{30}F_6IrN_5S_2$
Formula weight	914.98
T (K)	296(2)
Wavelength (Å)	0.71073
Crystal system	Monoclinic
Space group	$P2_1/n$
a (Å)	13.9038(13)

b (Å)	34.924(3)
c (Å)	15.0724(15)
α (deg)	90
β (deg)	92.347(2)
γ (deg)	90
V (Å^3)	7312.7(12)
Z	8
ρ_{calcd} (g/cm^3)	1.662
μ (Mo Kα) (mm^{-1})	3.831
F (000)	3600
Range of transm factors (deg)	1.473-25.010
Reflns collected	41033
Unique(R_{int})	12875(0.0563)
$R_1{}^a$, $wR_2{}^b$ [I > 2s(I)]	0.0440, 0.0995
$R_1{}^a$, $wR_2{}^b$ (all data)	0.0689, 0.1127
GOF on F^2	1.022

($R_1{}^a = \Sigma||F_o| - |F_c||/\Sigma|F_o|$)

($wR_2{}^b = [\Sigma w(F_o{}^2 - F_c{}^2)^2/\Sigma w(F_o{}^2)]^{1/2}$)

Table 2. Main bond lengths and angles of ***Ir$_{red}$***.

	Ir$_{red}$
Selected Bonds	Bond length (Å)
Ir-C(1)	2.002(7)
Ir-C(2)	1.995(7)
Ir-N(1)	2.045(5)
Ir-N(2)	2.036(6)
Ir-S(1)	2.4488(19)
Ir-S(2)	2.4499(19)
S(1)-C(3)	1.725(8)
S(2)-C(3)	1.719(7)
C(3)-N(3)	1.329(9)
Selected angles	(°)
C(1)-Ir-N(1)	79.0(2)
C(2)-Ir-N(2)	78.4(3)
S(1)-Ir-S(2)	71.42(7)
S(2)-C(3)-S(1)	112.2(4)
C(3)-S(2)-Ir	88.2(3)
C(3)-S(1)-Ir	88.1(3)
N(3)-C(3)-S(1)	124.2(6)

2.3.2 Thermogravimetric analysis

The thermal stability of ***Ir**red* values a lot for organic electroluminescent devices. By thermogravimetry (TG) method, we measured the thermal property of the Ir(III) complex. The TG curve in the Figure 11 (5% wt weight loss) is as high as 384°C, which indicates that the introduction of sulfur atoms in ancillary ligand can strongly affect the decomposition temperature of complex. Moreover, the high decomposition temperature of the complex indicates that it could be used in OLEDs.

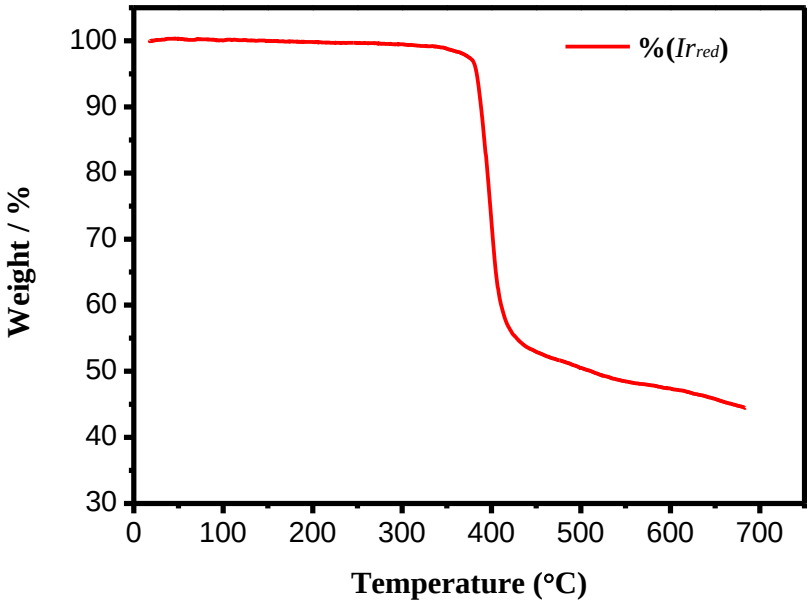

Figure 11. TG curve of ***Ir**red*.

2.3.3 Photophysical property of ***Ir**red*

As shown in Figure 12, the UV-Vis absorption and emission spectra of ***Ir**red* were measured in the dichloromethane solution (without oxygen) with a concentration of 5×10^{-5} mol/L. And, the relevant data are listed in Table 3.

The intense absorption bands below 400 nm arise from the spin-allowed intraligand π → π * transitions, and the relatively weak bands in the visible region (400-630 nm) can be assigned to the mixed ^{1}MLCT and ^{3}MLCT (metal-to-ligand charge-transfer) states, or LLCT (ligand-to-ligand charge-transfer) transition through strong spin-orbit coupling of iridium atom.

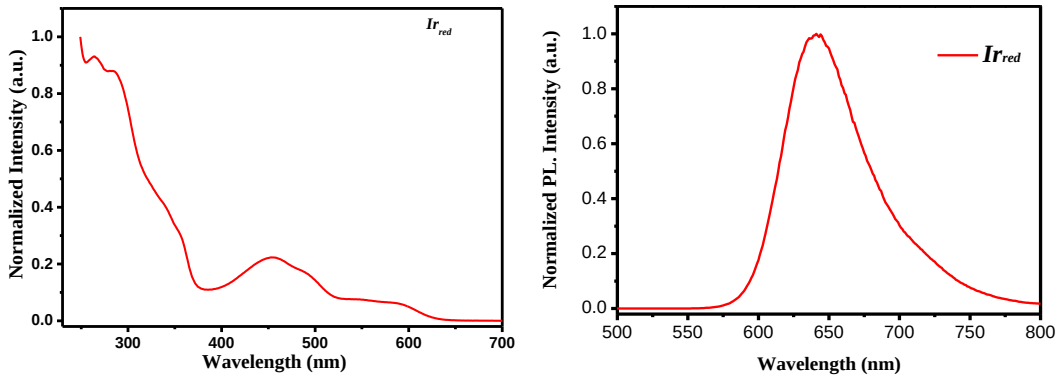

Figure 12. The absorption spectrum (left) and emission spectrum of ***Ir**red* (right).

Table 3. The Photophysical Properties of ***Ir**red*.

Complex	T_d (°C)[a]	Absorption (λ nm)[b]	Emission (λ_{max} nm)[b]	$\tau_{298\ K}$ (μs)[b]	Φ_P (%)[c]	E_T (eV)[d]	HOMO/LUMO (eV)[e]
***Ir**red*	384	263/285/453/592	641	1.41	58.3	2.04	-5.44/-3.19

[a] T_d: decomposition temperature (with 5% mass loss); [b] Determination at room temperature in dichloromethane solution (without oxygen), with a solution concentration of 5×10^{-5} mol/L; [c] Determination at room temperature with *fac*-Ir(ppy) as a reference material (Φ= 0.40) in dichloromethane solution; [d] The cyclic voltammetry curve and UV-Vis absorption spectrum were calculated with ferrocene as internal standard.

The PL quantum yield of ***Ir**red* was measured as 58.3%. In addition, the lifetime of ***Ir**red* is in the microsecond range (1.41 μs), which is indicative of the phosphorescent origin for the excited states in the case.

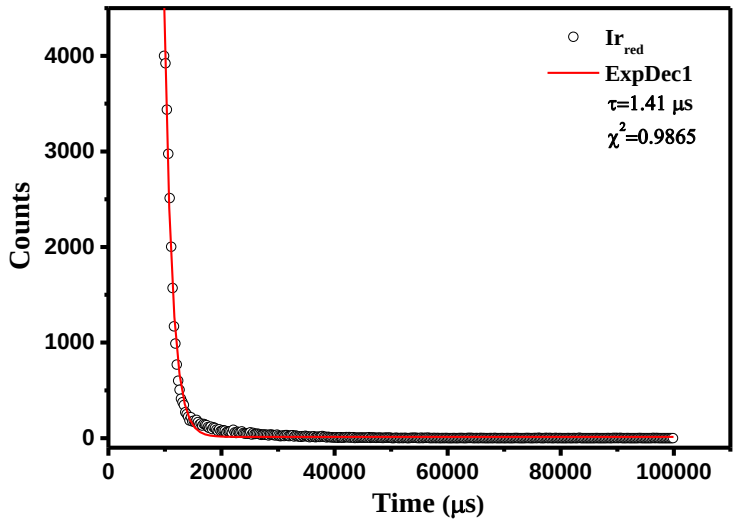

Figure 13. Lifetime curve of ***Ir**red*.

2.3.4 Electrochemistry and the theoretical calculation

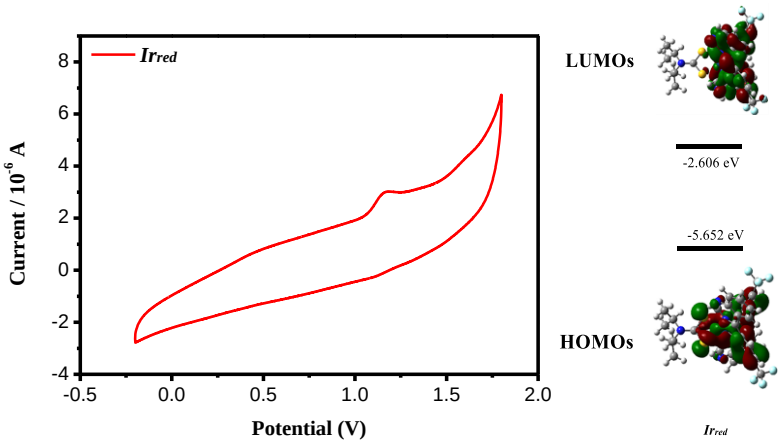

Figure 14. Cyclic voltammetric curve of ***Ir**red* (Left) and orbital electron density distributions of HOMO/LUMO (Right).

The HOMO / LUMO level values of the complex matter a lot to the design of OLEDs. In order to measure the HOMO/LUMO energy levels of ***Ir**red*, the electrochemical properties of the complex were studied by cyclic voltammetry in dichloromethane solution (without oxygen) with ferrocene as external standard and saturated potassium chloride calomel electrode as reference electrode. As shown in Figure 14 (left), the cyclic voltammetric curve of ***Ir**red* shows a strong oxidation peak, but the reduction peak is not obvious, displaying that the redox process of complex is irreversible. According to the peak value of oxidation with the equation of $E_{HOMO} = (E_{OX} + 4.8)$ eV, the HOMO level is calculated as -5.44 eV. Based on the HOMO level and spectral bandgap, the LUMO level is calculated to be -3.49 eV.

Table 4. The electronic cloud density distributions of ***Ir**red*

Complex	Orbital	Energy/eV (Calculated)	Energy/eV (experimental)	Composition (%)		
				Main ligand	Ir	Ancillary Ligand
***Ir**red*	HOMO	-5.65	-5.44	47.9	39.42	12.67
	LUMO	-2.61	-3.19	94.35	3.45	2.20

In order to understand the electronic states and orbital electron cloud density distribution of this complex, the density functional theory (DFT) calculation of complex was carried out by using the Gauss09 software and B3LYP method. The HOMO/LUMO level diagram and orbital electron cloud distribution were shown in Figure 14 (right).

The density distribution of electron cloud and the theoretical calculated energy level data are shown in Table 4. The C, H, N, S and F atoms are based on 6-31G (d, p) group, while the Ir atoms are based on LANL2DZ group. The solvent effect of dichloromethane is considered by using the Conductor Polarization Continuous Model (C-PCM). The electron clouds of the HOMO level of the complex are mainly distributed on the main ligand quinazoline (47.90%) and the *d* orbit of Ir (39.42%), while the contribution of the ancillary ligand is very small (12.67%). The electron clouds of the LUMO level are mainly distributed on the main ligand (94.35%), and a small contribution on the *d* orbit of Ir (3.45%) and the auxiliary ligand (2.20%). The calculated HOMO and LUMO levels of the complexes are almost in agreement with the measured values.

2.3.5 OLED performances

To illustrate their electroluminescence (EL) properties, typical OLED using the complex as an emitter was fabricated with ITO / HAT-CN (dipyrazino[2,3-f:2',3'-h]quinoxaline-2,3,6,7,10,11-hexacarbonitrile, 6 nm) / HAT-CN (0.2 wt%) : TAPC (di-[4-(*N*,*N*-ditolylamino) phenyl]cyclohexane, 50 nm) / ***Ir**red* (3 wt%) : 2,6DCzPPy (2,6-bis(3-(carbazol-9-yl)phenyl)pyridine, 10 nm) / Tm3PyP26PyB (1,3,5-tris(6-(3-(pyridin-3-yl)phenyl)pyridin-2-yl) benzene, 60 nm) / LiF (1 nm) / Al (100 nm) is named as **Dev1**.

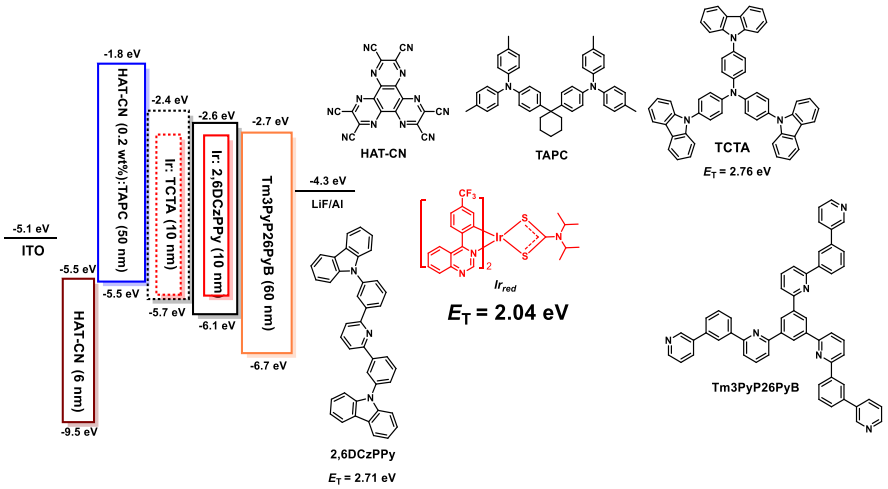

Scheme 2. Energy level diagram of HOMO and LUMO levels (relative to vacuum level) for materials investigated in this work and their molecular structures.

As shown in Scheme 2, HAT-CN and LiF serve as hole- and electron-injecting interface modified materials, respectively. The bipolar 2,6DCzPPy is chosen as the host material. The TAPC with high HOMO level (-5.5 eV) acts as the hole-transport media, and the layer of TAPC doped with 0.2 wt% HAT-CN is to further enhance the hole-transporting ability. While Tm3PyP26PyB with low LUMO level (-2.7 eV) is used as electron-accepting and electron-transport material. The HOMO and LUMO levels of ***Ir**red* is embedded between those of 2,6DCzPPy (HOMO = 6.10 eV, LUMO = 2.60 eV). Thus, efficient energy transfer from the host to Ir(III) complex would be occurred in the emitting layer (EML). Furthermore, holes and electrons can be injected to HOMO and LUMO levels of host material or trapped by the dopant directly owing to the difference of the HOMO/LUMO levels between ***Ir**red* and the host material. And in the bipolar host 2,6DCzPPy the excitons can be easily formed and distributed more balanced, which is helpful to reduce the turn-on voltage of the device, which was optimized and displays the best EL performances at 3 wt% doping concentration. The EL spectrum, current density (J) - voltage (V) - luminance (L), current efficiency (η_c) and power efficiency (η_p) versus luminance, and EQE as a function of luminance characteristics of the devices are displayed in Figure 15. And the parameters of these devices are summarized in Table 5.

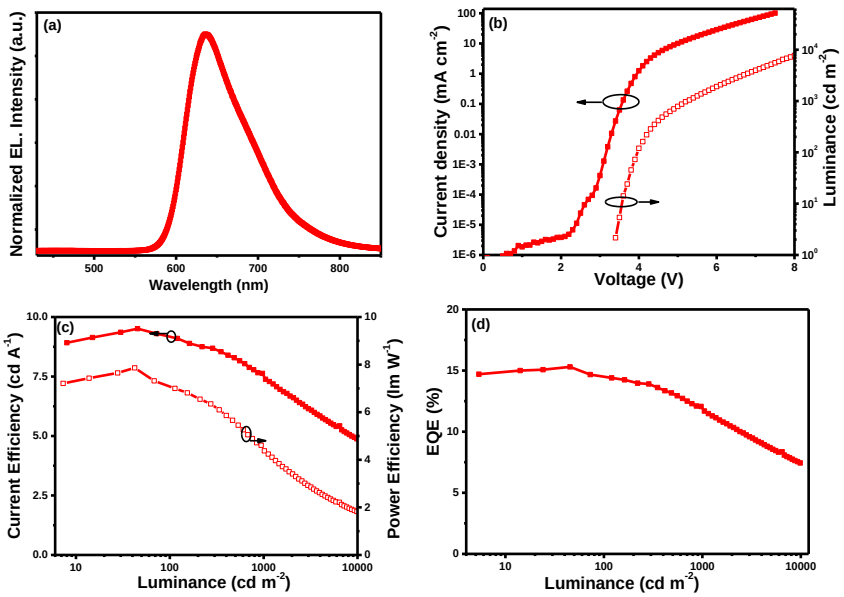

Figure 15. Characteristics of single-emitting-layer device **Dev1**: (a) EL spectrum, (b) J – V - L curves, (c) η_c – L - η_p curves and (d) EQE - L curve.

Table 5. The key EL data of device **Dev1**.

Device	$V_{turn\text{-}on}$[a] (V)	L_{max} (cd m^{-2})	$\eta_{c,max}$ (cd A^{-1})	$\eta_{ext,max}$ (%)	$\eta_{p,max}$ (lm W^{-1})	η_c[b] (cd A^{-1})	η_{ext}[b] (%)
Dev1	3.4	26 490	9.51	15.3	7.86	7.38	11.69

Figure 15(a) shows the normalized EL spectrum of **Dev1** measured at the current of 1 mA with peak at about 636 nm, which is very close to the PL spectrum of the ***Ir**red*, indicating that the EL emission of the device originates from the triplet excited state of the phosphor in which all the Commission Internationale de 1'Eclairage (CIE) color coordinate falls in the red region. The device Dev1 shows EL performances with the maximum luminance (L_{max}) above 26000 cd m^{-2}, the peak current efficiency ($\eta_{c,max}$) of 9.81 cd A^{-1}, the peak power efficiency ($\eta_{p,max}$) of 7.86 lm W^{-1} and a maximum external quantum efficiency (EQE_{max}) of 15.30%.

Summarized from the investigated results, the superior device properties may result from the following facts: Firstly, dithiocarbamate with electron-donating moiety and the nitrogen frame of the 4-(4-(trifluoromethyl)phenyl)quinazoline were applied as the ligands for stable Ir(III) complex with bipolar properties, which may contribute to a wider recombination area and a more balanced distribution for the excitons. Secondly, the coordination capability of sulfur atom with iridium atom is strong, the stable dithiolate compounds can reduce the work function of the emitter and the threshold electric field. The dithiocarbamate can lower the LUMO energy level of ***Ir**red*, and the electron transport property can also be benefited.

2.4 Conclusion

Due to the sulfur atoms in the dithioformate ancillary ligand, a red Ir(III) complex with 4-(4-trifluoromethylphenyl)quinazoline as main ligand was synthesized at room temperature in few minutes. The single crystal analysis confirmed its molecular structure. Theoretical calculations show that the HOMO-level electron clouds of the complex mainly distribute in the main ligands quinoxaline and *d* orbital of the Ir atom, and the LUMO-level electron clouds mainly distribute in the main ligand. The emission

peak reaches 641 nm with a quantum efficiency in the solution of 58.3%, and the lifetime of the excited state is also in microsecond order. The complex has electron-donating 4-(4-trifluoromethylphenyl)quinazoline group and electron-withdrawing iisopropylamine group, which means that it has bipolar ability, thus largely improving the device efficiency and reducing the efficiency roll-off. Using this complex as emitter, the single-layer OLED shows good performances with a L_{max} above 26000 cd m^{-2}, a $\eta_{c,max}$ of 9.81 cd A^{-1} and an EQE_{max} of 15.30%. From the above discussion, we can find out that with the sulfur containing dithioformate ligand can synthesize the Ir(III) complex efficiently and reduce the cost.

3. Rapid synthesis of a green iridium(III) complex with four-membered Ir-S-C-S chelating ring at room temperature

3.1 Experimental

3.1.1 Reagents needed:

2,4-*bis*(trifluoromethyl)phenylboronic acid, 2-bromopyridine, diisopropylamine, LiOH • H_2O, benzene, carbon disulfide, $IrCl_3$, anhydrous THF, 2-ethoxyethanol ($EtOCH_2CH_2OH$) and $Pd(PPh_3)_4$.

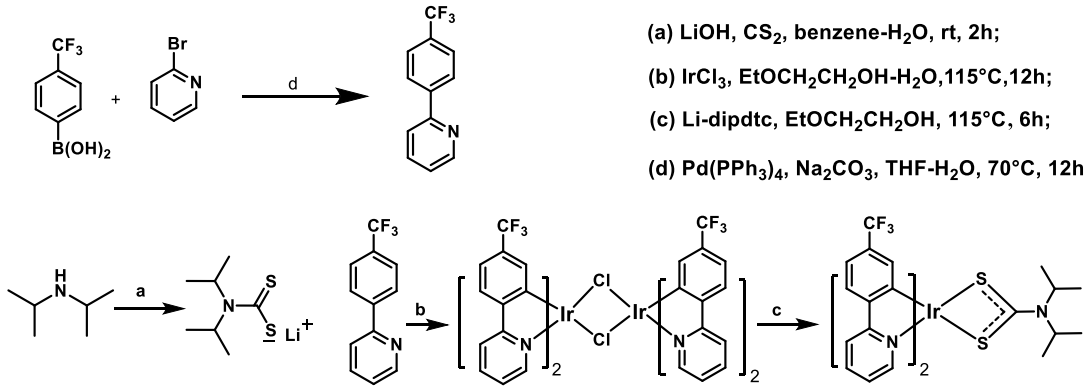

Scheme 3. Synthetic route of ligands and green Ir(III) complex.

3.1.2 Synthesis of 2-[4-(trifluoromethyl)phenyl]pyridine

Put 2,4-*bis*(trifluoromethyl)phenylboronic acid (2.5 mmol, 0.48 g), 2-bromopyridine (2.5 mmol, 0.42 g) and $Pd(PPh_3)_4$ (2.5 mmol, 2.8 g) into the reaction container under nitrogen protection and heat the container in oil (70 °C) for 12h. Separate the liquid

mixture after extraction to get the 2-[4-(trifluoromethyl)phenyl]pyridine(1.0 mmol) with a yield of 40%.

3.1.3 Synthesis of chloride bridge dimmer.

2-[4-(trifluoromethyl)phenyl]pyridine and $IrCl_3$ are put into three-mouth flask like the portion of ***Ir**red*. Add $EtOCH_2CH_2OH$ (12 mL), water (3 mL) into the flask and keep heating at 115 ^oC for 12h. After cooling down and water was added to form the precipitate, which was filtrated and washed with dichloromethane to get the chloride bridge dimmerwith a yield of 40%.

3.1.4 Synthesis of the complex

The chloride bridge dimmer, dithioformate and $EtOCH_2CH_2OH$ (10 mL) are added into the three-mouth flask under nitrogen, which was stirred constantly for 5 minutes. The solution was extracted with CH_2Cl_2 and water, dried with anhydrous Na_2SO_4. After removing the solvent in vacuum, the residue was purified by chromatography with eluent (CH_2Cl_2 : petroleum ether = 2:1). Due to the green light it gives off under UV light, we name the complex ***Ir**green*.

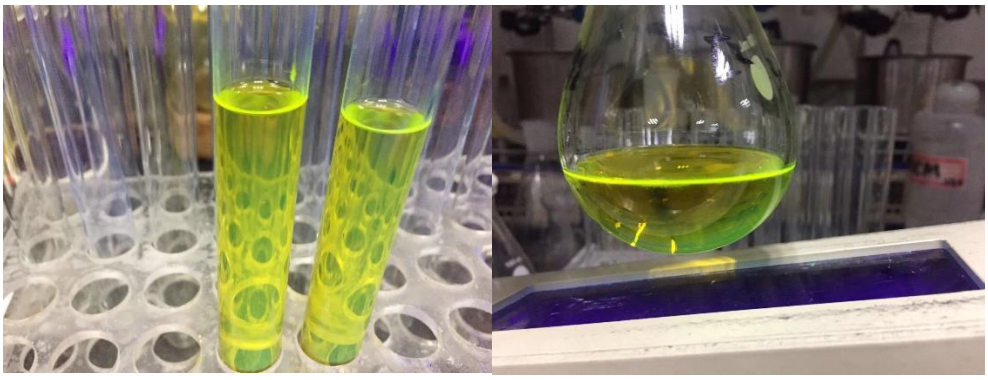

Figure 16. ***Ir**green* in the solution under UV light.

3.2 Results and discussion

3.2.1 Analysis of the structure of single ***Ir**green* crystal.

The single crystal was obtained by vacuum sublimation and X-ray diffraction measurements was carried out. The ellipsoid structure is shown in Figure 17. Crystal parameters and bond length and bond angle data are shown in the Table 6 and 7.

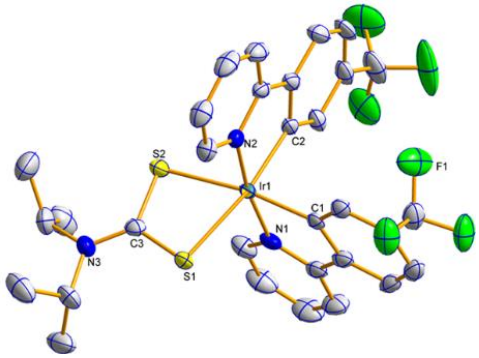

Figure 17. The ellipsoid structure of the complex ***Ir**green* (hydrogen omitted),(CCDC No. 1832358). Ellipsoids are drawn at 50% probability level.

Table 6. Crystallographic data of the complex

	***Ir**green*
Formula	$C_{31}H_{28}F_6IrN_3S_2$
Formula weight	812.88
T (K)	296(2)
Wavelength (Å)	0.71073
Crystal system	Orthorhombic
Space group	Pbcn
a (Å)	15.7090(7)
b (Å)	19.7575(9)
c (Å)	21.8169(9)
α (deg)	90
β (deg)	90
γ (deg)	90
V (Å^3)	6771.3(5)
Z	8
ρ_{calcd} (g/cm^3)	1.595
μ (Mo Kα) (mm^{-1})	4.124
F (000)	3184
Range of transm factors (deg)	2.263-25.008
Reflns collected	46788
Unique(R_{int})	5952(0.0355)
$R_1{}^a$, $wR_2{}^b$ [I > 2s(I)]	0.0212, 0.0506
$R_1{}^a$, $wR_2{}^b$ (all data)	0.0287, 0.0547
GOF on F^2	1.075

($R_1{}^a = \Sigma||F_o| - |F_c||/\Sigma F_o|$)

($wR_2^b = [\Sigma w(F_o^2 - F_c^2)^2/\Sigma w(F_o^2)]^{1/2}$)

Table 7. Main bond lengths and angles of the complex

	Ir_{green}
Selected bonds	Bond length (Å)
Ir-C(1)	2.010(3)
Ir-C(2)	2.015(3)
Ir-N(1)	2.055(3)
Ir-N(2)	2.047(2)
Ir-S(1)	2.4552(7)
Ir-S(2)	2.4456(8)
S(1)-C(3)	1.735(3)
S(2)-C(3)	1.723(3)
C(3)-N(3)	1.323(4)
Selected angles	(°)
C(1)-Ir-N(1)	80.2(11)
C(2)-Ir-N(2)	80.24(11)
S(1)-Ir-S(2)	71.36(3)
S(2)-C(3)-S(1)	111.50(18)
C(3)-S(2)-Ir	88.74(11)
C(3)-S(1)-Ir	88.18(11)
N(3)-C(3)-S(1)	123.5(2)

As shown in Figure 17, the complex ***Ir**green* has distorted octahedral coordination geometry around iridium center by three chelating ligands, in which the N-Ir-N angle for the complex is 172.2°. The four-membered Ir-S-C-S backbone could cause the structure to significantly more acute S-Ir-S bite angle (71.4°) than that for the larger five-membered or six-membered heterocycles based on such as pic, acac group and their derivatives. The Ir-C bond lengths are 2.010-2.015 Å and the Ir-N bond lengths are 2.047-2.055 Å, which are slightly shorter than the Ir-S bonds (2.4456-2.4552 Å). The Ir-C and Ir-N bond lengths are similar to those reported in other mononuclear complexes with $(C^N)_2Ir$ fragment. These facts indicate that -1 charge of *N*,*N*-diisopropyldithiocarbamate is delocalized over both sulfur atoms. The two coordinated S atoms of ancillary ligand reside in the equatorial plane *trans* to the metalated C atoms of the three main ligands.

3.2.2 Thermogravimetric analysis

As mentioned before, the thermal stability of the complex is very important to the

OLED operation. From the DSC curve in Figure 18 it's clear that the melting point of ***Ir**green* is 323 °C. In the TG curve (right), its thermal decomposition temperatures (T_d, corresponding to 5% weight loss) is 334°C. The two figures show the thermal stability of ***Ir**green* is very good, and it has potential in OLED service.

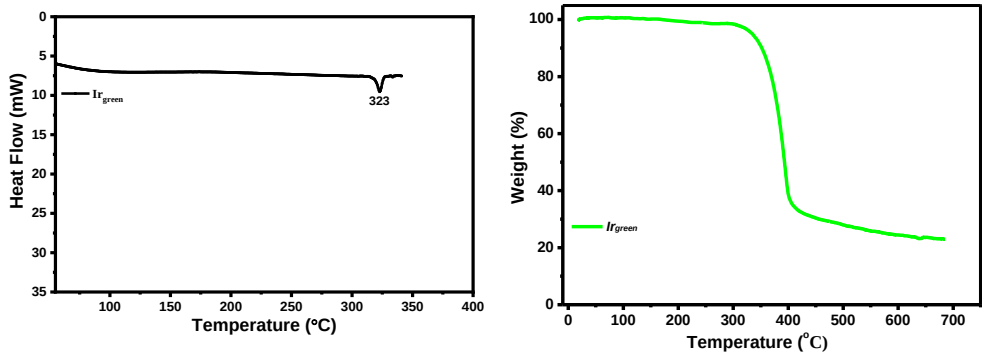

Figure 18. DSC (left) and TG (right) curves of ***Ir**green*.

3.2.3 Photophysical property of ***Ir**green*

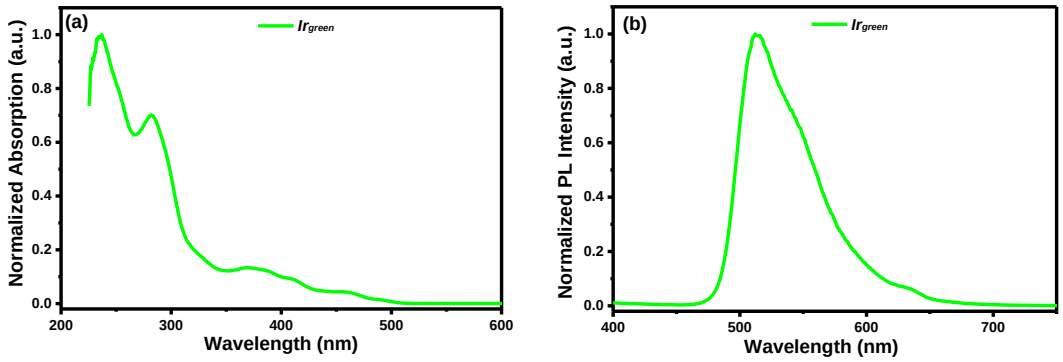

Figure 19. The UV-vis absorption (a) and emission (b) spectra of the complex in dichloromethane without oxygen (5×10^{-5} M) at room temperature.

The UV-Vis absorption and emission spectra of ***Ir**green* were measured in the dichloromethane solution (without oxygen) with a concentration of 5×10^{-5} mol/L are shown in Figure 19.

The intense absorption bands below 350 nm arise from the spin-allowed intraligand π→π* transitions, and the relatively weak bands in the visible region (350-530 nm) can be assigned to the mixed ^{1}MLCT and ^{3}MLCT (metal-to-ligand charge-transfer) states,

or LLCT (ligand-to-ligand charge-transfer) transition through strong spin-orbit coupling of iridium atom. The obvious changes of emission wavelength coincide with the large difference of energy gaps by the electrochemical analysis and the theoretical calculations (Table 8).

Table 8. Photophysical data of ***Ir$_{green}$***.

Complex	T_m [a] (°C)	T_d [b] (°C)	λ_{abs} [c] (nm)	λ_{em} [c] (nm)	Φ [d] (%)	τ [c] (μs)
Ir$_{green}$	323	334	235/281/373	513	71.6	1.38

[a] T_m: Melting point; [b] T_d: Decomposition temperature (with 5% mass loss); [c] Determination at room temperature in dichloromethane solution (without oxygen), with a solution concentration of 5×10^{-5} mol/L; [d] Determination at room temperature with *fac*-Ir(ppy) as a reference material (Φ= 0.40) in dichloromethane solution.

The PL quantum yield of the ***Ir$_{green}$*** was measured as 71.6%, and the lifetime is in the range of microseconds. And the relatively short lifetime is key to the device performance in which the abundant excitons produced instantaneously by electrical excitation can effectively decay.

3.2.4 Electrochemistry and the theoretical calculations

In order to determine the HOMO/LUMO levels of ***Ir$_{green}$***, the electrochemical property of ***Ir$_{green}$*** was investigated by cyclic voltammetry in deaerated CH_2Cl_2, relative to an internal ferrocenium/ferrocene reference (Fc^+/Fc) (Figure 20). According to the equation of $E_{HOMO} = -(E_{ox} - E_{Fc/Fc+} + 4.8)$ eV, the HOMO energy level (E_{HOMO}) of ***Ir$_{green}$*** was obtained. Based on the E_{HOMO} and optical band gap calculated by the equation of $\Delta E_{bandgap}= 1240/\lambda_{abs\text{-}onset}$, the LUMO energy level was also obtained.

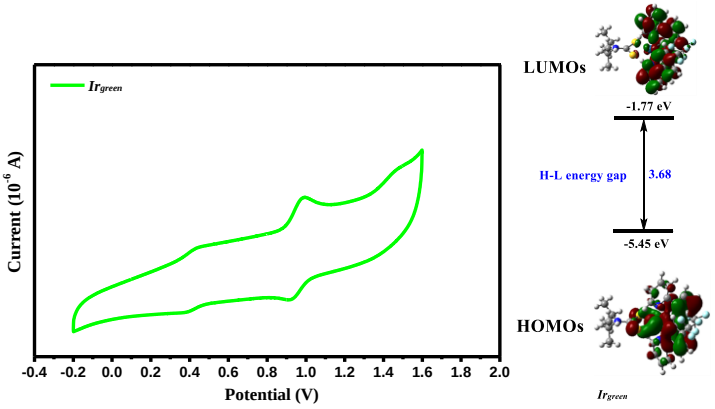

Figure 20. Cyclic voltammogram curve of ***Ir$_{green}$*** (left) and molecular orbital diagram for the HOMOs/LUMO of the complex calculated in CH_2Cl_2 (right).

To determine the HOMO and LUMO distribution of ***Ir$_{green}$***, the density functional theory (DFT) calculation was also performed, and the details of the theoretical calculations are shown below. As shown in the Table 9, the HOMO orbital of the *Ir$_{green}$* mostly located on the main ligand (47.90%) together with *d*- orbital of iridium atom (48.11%) with a small portion of the *N*,*N*-diisopropyldithiocarbamate (8.79%). A larger scale distribution of electron cloud on the iridium atom indicates an efficient MLCT of the phosphorescent complex, crucial to the high PL quantum efficiency. The LUMO are mostly distributed over the π* orbital of the main ligand (92.83%) and to a small extent on Ir *d* orbital (3.94%) and ancillary ligand (3.23%). As the main ligand change, the changed calculated energy gap (3.68) correlates well with the electrochemical results.

Table 9. The electronic cloud density distribution of ***Ir$_{green}$***.

Complex	Orbital	Energy/eV (Calculated)	Energy/eV (experimental)	Composition (%)		
				Main Ligands	Ir	Ancillary Ligands
Ir$_{green}$	HOMO	-5.45	-5.25	47.9	48.18	8.79
	LUMO	-1.77	-2.8	92.83	48.18	3.23

3.2.5 OLED performance

Since the OLED device with single emissive layer has been examined before, in this section we would mainly discuss the OLED with double emissive layers with the configuration of ITO / HAT-CN (dipyrazino[2,3-f:2',3'-h]quinoxaline-2,3,6,7,10,11-hexacarbonitrile, 5 nm) / TAPC (*di*-[4-(*N*,*N*-ditolylamino)phenyl]cyclohexane, 50 nm) / ***Ir$_{green}$*** (x wt%) : TCTA (4,4',4''-tris(carbazol-9-yl)triphenylamine, 8 nm) / ***Ir$_{green}$*** (x wt%) : 2,6DCzPPy (2,6-*bis*(3-(carbazol-9-yl)phenyl)pyridine, 8 nm) / TmPyPB (1,3,5-*tri*[(3-pyridyl)-phen-3-yl]benzene, 50 nm) / LiF (1 nm) / Al (100 nm) named as **Dev2**. As shown in Figure 22, the materials of HAT-CN and LiF served as hole- and electron-injecting interface modified materials, respectively. The bipolar material 2,6DCzPPy and the hole-transporting material TCTA were chosen as host materials, respectively.

The stepwise changed HOMO energy levels of TAPC (-5.5 eV), TCTA (-5.7 eV) and 2,6DCzPPy (-6.1 eV) are beneficial for the hole injection and transport. Similarly, it is also beneficial for the injection and transport of electrons owing to the gradual changed LUMO energy levels of TmPyPB (-2.7 eV), 2,6DCzPPy (-2.6 eV) and TCTA (-2.4 eV). Additionally, the triplet state (2.34) of the ***Ir$_{green}$*** is within the 2,6DCzPPy, which is helpful to inhibit the energy reversion from the guest to the host. Thus, holes and electrons will be distributed in more balanced emissive layers and the exciton recombination zone is expected to be broadened. Furthermore, the HOMO energy level of TmPyPB is 0.6 eV lower than that of 2,6DCzPPy and the LUMO energy level of TAPC is 0.6 eV higher than that of TCTA, which would result in well conformed exciton (hole-electron pair) within emissive layers and the triplet exciton quenching avoided effectively.

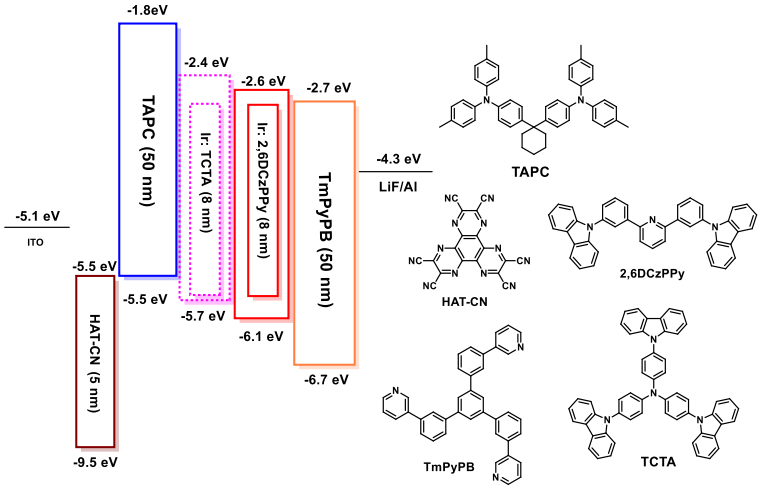

Scheme 4. Energy level diagram of HOMO and LUMO levels (relative to vacuum level) for materials investigated in this work and their molecular structures.

The electroluminescence (EL) spectrum, current density (*J*)-voltage (*V*)-luminance (*L*), current efficiency (η_c) and power efficiency (η_p) versus luminance, and EQE as a function of luminance characteristics of the device are displayed in Fig. 22(a)-(d), and the parameters of the device is summarized in Table 10. Figure 22(a) shows the normalized EL spectrum of the device measured at the voltage of 5 V with peak at about 510 nm for device **Dev 2**, which is very close to the PL spectrum of ***Ir$_{green}$***, indicating that the EL emission of the device originates from the triplet excited states of the phosphor.

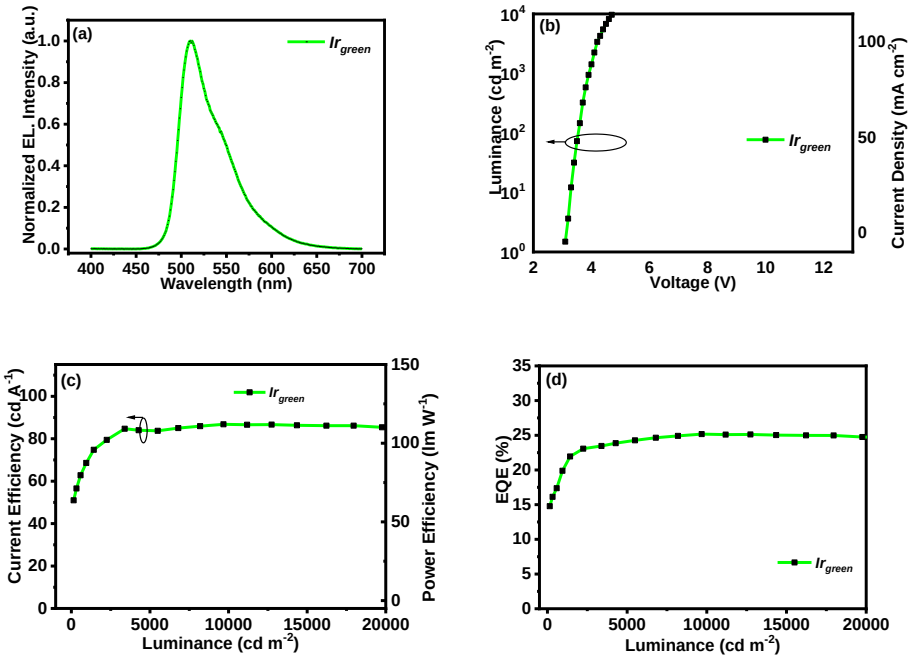

Figure 21. Device characteristics: (a) EL spectrum, (b) *J*-*V*-*L*, (c) η_c-*L*-η_p and (d) EQE-*L* curves of **Dev 2**.

The **Dev 2** (Φ_P of ***Ir*$_{green}$** is 71.6%) at a doping concentration of 8 wt% shows good EL performances with the maximum luminance (L_{max}) above 33466 cd m^{-2}, the peak current efficiency ($\eta_{c,max}$) of 86.81 cd A^{-1}, the peak power efficiency ($\eta_{p,max}$) of 59.85 lm W^{-1} and a maximum external quantum efficiency (EQE$_{max}$) of 25.17% with CIE coordinates of (0.253, 0.634).

Table 10. EL performances of the device.

Device	$V_{turn\text{-}on}$ [a)] (V)	L_{max} (cd m^{-2})	$\eta_{c,max}$ (cd A^{-1})	$\eta_{ext,max}$ (%)	$\eta_{p,max}$ (lm W^{-1})	η_c [b)] (cd A^{-1})	η_{ext} [b)] (%)	CIE [c)] (x, y)
Dev 2	3.1	33466	86.81	25.17	59.85	86.18	24.92	(0.253, 0.634)

[a)] Applied voltage recorded at a luminance of 1 cd m^{-2}; [b)] Recorded at 10000 cd m^{-2}; [c)] Measured at driving voltage of 5 V.

3.3 Conclusion

Due to the sulfur atoms in the dithioformate ancillary ligand, a green Ir(III) complex with 2-[4-(trifluoromethyl)phenyl]pyridine as main ligand was synthesized at room temperature in five minutes. The single crystal analysis confirmed its molecular structure. Theoretical calculations show that the HOMO-level electron clouds of the complex mainly distribute in the main ligands quinoxaline and *d* orbital of the Ir atom,

and the LUMO-level electron clouds mainly distribute in the main ligand. The emission peak reaches 513 nm with a quantum efficiency in the solution of 71.6%, and the lifetime of the excited state is also in microsecond order. Using this complex as emitter, the OLED with double emissive layers shows good performances with a L_{max} above 33466 cd m^{-2}, a $\eta_{c,max}$ of 86.81 cd A^{-1} and an EQE_{max} of 25.17%. From the above discussion, we can find out that with the sulfur containing dithioformate ligand can be used as a potential ligand for synthesis of the Ir(III) complex efficiently and reduce the cost.

4. Conclusions

In summary, with use of dithioformate ancillary ligand containing sulfur atoms, we successfully constructed versatile iridium complexes rapidly at room temperature. By synthesizing these complexes at room temperature in mere minutes, costs of the OLEDs are successfully reduced. More interestingly, we showed the Basic thermal, photophysical, structural properties and the performance in devices. Since the high capabilities of these four-membered-ring complexes, it is reasonable to speculate that these multifunctional material might find potentials in the area of display.

References:

[1] a) S. Lamansky, P. Djurovich, D. Murphy, F. Abdel-Razzaq, H.-E. Lee, C. Adachi, P. E. Burrows, S. R. Forrest, M. E. Thompson, *J. Am. Chem. Soc.* **2001**, *123*, 4304; b) Z.-Q. Chen, Z.-Q. Bian, C.-H. Huang, *Adv. Mater.* **2010**, *22*, 1534; c) S. Chen, G. Tan, W.-Y. Wong, H.-S. Kwok, *Adv. Funct. Mater.* **2011**, *21*, 3785; d) K.-Y. Lu, H.-H. Chou, C.-H. Hsieh, Y.-H. O. Yang, H.-R. Tsai, H.-Y. Tsai, L.-C. Hsu, C.-Y. Chen, I. C. Chen, C.-H. Cheng, *Adv. Mater.* **2011**, *23*, 4933; e) H.-H. Chou, Y.-K. Li, Y.-H. Chen, C.-C. Chang, C.-Y. Liao, C.-H. Cheng, *ACS. Appl. Mater. Interfaces* **2013**, *5*, 6168; f) X. Yang, N. Sun, J. Dang, Z. Huang, C. Yao, X. Xu, C.-L. Ho, G. Zhou, D. Ma, X. Zhao, W.-Y. Wong, *J. Mater. Chem. C* **2013**, *1*, 3317; g) X. Yang, G. Zhou,

W.-Y. Wong, *J. Mater. Chem. C* **2014**, *2*, 1760.

[2] a) H. Uoyama, K. Goushi, K. Shizu, H. Nomura, C. Adachi, *Nature*, **2012**, *492*, 234; b) M. Y. Wong, E. Zysman-Colman, *Adv. Mater*. **2017**, *29*, 1605444; c) Y. Im, M. Kim, Y. J. Cho, J.-A Seo, K. S. Yook, J. Y. Lee, *Chem. Mater*. **2017**, *29*, 1946; d) Z. Yang, Z. Mao, Z. Xie, Y. Zhang, S. Liu, J. Zhao, J. Xu, Z. Chi, M. P. Aldred, *Chem. Soc. Rev*. **2017**, *46*, 915.

[3] a) Baldo, M. A.; O'Brien, D. F.; You Y.; Shoustikov, A.; Sibley, S.; Thompson, M. E.; Forrest, S. R. *Nature* **1998**, *395*, 151-154; b) Baldo, M A.; Lamansky, S.; Burrows, P. E.; Thompson, M. E.; Forrest, S. R. *Appl. Phys. Lett*. **1999**, *75*, 4-6; c) Thompson, M. E.; Burrows, P. E.; Forrest, S. R. *Cur. Opinion Solid State Mater. Sci*. **1999**, *4*, 369.

[4] a) M. A. Baldo , S. Lamansky , P. E. Burrows , M. E. Thompson , S. R. Forrest , *Appl. Phys. Lett*. **1999** , *75* , 4 ; b) R. J. Holmes , S. R. Forrest , Y. J. Tung , R. C. Kwong , J. J. Brown , S. Garon , M. E. Thompson , *Appl. Phys. Lett.* **2003** , *82* , 2422 ; c) S. Tokito , T. Iijima , Y. Suzuri , H. Kita , T. Tsuzuki , F. Sato , *Appl. Phys. Lett.* **2003** , *83* , 569 ; d) J. Li , P. I. Djurovich , B. D. Alleyne , M.Yousufuddin , N. N. Ho , J. C. Thomas , J. C. Peters , R. Bau , M. E. Thompson , *Inorg. Chem*. **2005** , *44* , 1713 ; e) S. Okada , K. Okinaka , H. Iwawaki , M. Furugori , M. Hashimoto , T. Mukaide , J. Kamatani , S. Igawa , A. Tsuboyama , T. Takiguchi , K. Ueno , *Dalton Trans.* **2005** , *9* , 1583 ; f) Y.-Y. Lyu, Y. Byun, O. Kwon, E. Han, W. S. Jeon, R. R. Das, K. Char, *J. Phys. Chem. B* **2006** , *110* , 10303 ; g) C.-H. Yang, Y.-M. Cheng, Y. Chi, C.-J. Hsu, F.-C. Fang, K.-T. Wong, P.-T. Chou, C.-H. Chang, M.-H. Tsai, C.-C. Wu, *Angew. Chem. Int. Ed*. **2007**, *46*, 2418; h) G. J. Zhou, W. Y. Wong, B. Yao, Z. Y. Xie, L. X. Wang, *Angew. Chem. Int. Ed*. **2007**, *46*, 1149; i) C. L. Ho, W. Y. Wong, Q. Wang, D. G. Ma, L. X. Wang, Z. Y. Lin, *Adv. Funct. Mater.* **2008**, *18*, 928; j) C.-F. Chang, Y.-M. Cheng, Y. Chi, Y.-C. Chiu, C.-C. Lin, G.-H. Lee, P.-T. Chou, C.-C. Chen, C.-H. Chang, C.-C. Wu, *Angew. Chem. Int. Ed*. **2008**, *47*, 4542.

[5] Y.-C Zhu, L. Zhou, H.-Y Li, Q.-L. Xu, M.-Y. Teng, Y.-X. Zheng, J.-L. Zuo, H.-J. Zhang, X.-Z. You, *Adv. Mater*., **2011**, *23*, 4041.

[6] a) S.-J. Ye, M.-F. Wu, C.-T. Chen, Y.-H. Song, Y. Chi, M.-H. Ho, S.-F. Chen, C. H.

Chen, *Adv. Mater.* **2005**, *17*, 285; b) S.-Y. Takizawa, H. Echizen, J. Nishida, T. Tsuzuki, S. Tokito, Y. Yamashita, *Chem. Lett.* **2006**, *35*, 748; c) C.-H. Yang, Y.-M. Cheng, Y. Chi, C.-J. Hsu, F.-C. Fang, K.-T. Wong, P.-T. Chou, C.-H. Chang, M.-H. Tsai, C.-C. Wu, *Angew. Chem. Int. Ed.* **2007**, *46*, 2418; d) S. H. Kim, J. Jang, S. J. Lee, J. Y. Lee, *Thin Solid Films* **2008**, *517*, 722; e) K. S. Yook, S. O. Jeon, C. W. Joo, J. Y. Lee, *Org. Electron.* **2009**, *10*, 170; f) H. Seo, K. Yoo, M. Song, J. S. Park, S. Jin, Y. I. Kim, J. Kim, *Org. Electron.* **2010**, *11*, 564; g) S. O. Jeon, S. E. Jang, H. S. Son, J. Y. Lee, *Adv. Mater.* **2011**, *23*, 1436.